Title: BEHAV3D Tumor Profiler to map heterogeneous cancer cell behavior in the tumor microenvironment

Emilio Rios-Jimenez*[1], Anoek Zomer*[2,3], Raphael Collot[2,3], Mario Barrera Román[2,3], Sandra F. Archidona[1], Hendrikus C.R. Ariese[2,3], Ravian L. van Ineveld[2,3], Michiel Kleinnijenhuis[2,3], Nils Bessler[2,3], Hannah Johnson[2,3], Caleb A. Dawson[4,5,6], Anne Rios[2,3] #, Maria Alieva[1] #.

* Equal contribution

Shared last authorship

Affiliations:

[1]Institute for Biomedical Research Sols-Morreale (IIBM), Spanish National Research Council-Universidad Autónoma de Madrid, Madrid, Spain.

[2]Princess Máxima Center for Pediatric Oncology, Utrecht, the Netherlands.

[3]Oncode Institute, Utrecht, the Netherlands.

[4]ACRF Cancer Biology and Stem Cells Division, The Walter and Eliza Hall Institute of Medical Research, Parkville, VIC 3052, Australia.

[5]Immunology Division, The Walter and Eliza Hall Institute of Medical Research, Parkville, VIC 3052, Australia.

[6]Department of Medical Biology, The University of Melbourne, Parkville, VIC 3010, Australia

Abstract

Intravital microscopy (IVM) enables live imaging of animals at single-cell level, offering essential insights into cancer progression. This technique allows for the observation of single-cell behaviors within their natural 3D tissue environments, shedding light on how genetic and microenvironmental changes influence the complex dynamics of tumors. IVM generates highly complex datasets that often exceed the analytical capacity of traditional uni-parametric approaches, which can neglect single-cell heterogeneous in vivo behavior and limit insights into microenvironmental influences on cellular behavior. To overcome these limitations, we present BEHAV3D Tumor Profiler (BEHAV3D-TP), a computational framework that enables unbiased single-cell classification based on a range of morphological and dynamic single cell features. BEHAV3D-TP integrates with widely used 2D and 3D image processing pipelines, enabling researchers without advanced computational expertise to profile cancer and healthy cell dynamics in IVM data. Here, we apply BEHAV3D-TP to study diffuse midline glioma (DMG), a highly aggressive pediatric brain tumor characterized by invasive progression. By extending BEHAV3D-TP to incorporate tumor microenvironment (TME) data from IVM or fixed correlative imaging, we demonstrate that distinct migratory behaviors of DMG cells are associated with specific TME components, including tumor-associated macrophages and vasculature. BEHAV3D-TP enhances the accessibility of computational tools for analyzing the complex behaviors of cancer cells and their interactions with the TME in IVM data.

INTRODUCTION

Cancer is a complex disease driven by a sequence of genetic and microenvironmental changes. As a result, tumors comprise many different cell populations that are in constant evolution[1] . This tumor heterogeneity has important biological and clinical implications as it differentially promotes key characteristics of individual cancer cells, including proliferation, invasion, and drug resistance [2]. Yet, we are far from fully understanding all the dynamic and bi-directional interactions in heterogeneous tumors, and how these interactions influence cancer cell behavior at the single-cell level. Emerging single-cell technologies and analysis tools provide a new opportunity to profile individual cells within tumors. For example, recent spatial transcriptomic and proteomic profiling provides evidence for the existence of multiple distinct microenvironmental niches within one tumor [3]. However, these techniques can only provide static information and make use of thin tissue sections that are only one cell layer thick. To investigate the real-time behavior of individual cells intravital microscopy (IVM) has been developed to study tumor cell behavior evolution over time but also in their three-dimensional native tissue environment.

IVM is a technique used to capture both spatial and temporal information at a single-cell level in living animals. Over the past years, it has provided many new insights into the dynamics of tumor heterogeneity and the development of therapy resistance [4–15] . For example, intravital imaging of mouse breast cancer models revealed that only a small portion of tumor cells is motile [15], and that fast- and slow-migrating cells are present in distinct regions of the tumor [7,16]. Moreover, additional heterogeneity exists among migrating tumor cells that can, for instance, move randomly or directionally relative to other tumor cells and/or surrounding healthy tissue [7]. However, traditional IVM analyses have considered cancer cells or the tumor microenvironment (TME) as a homogeneous population, thereby ignoring heterogeneity at the single-cell level and the influence of the local microenvironment, where interactions between neighboring cells may affect cellular behavior. To address these complexities, recent studies have used unbiased approaches using morpho-kinetic parameters derived from live *in vitro*[17] or *in vivo* imaging to classify cells and explore the single-cell behavioral landscape as an additional omic layer [18–20]. In line with this concept of characterizing cellular dynamic properties for cell classification, we have previously developed an analytical platform termed BEHAV3D [19,21] allowing to perform behavioral phenotyping of engineered T cells targeting cancer. While BEHAV3D was initially developed to analyze T cell migratory behavior under controlled in vitro conditions, we sought to expand its application to investigate tumor cell behaviors in IVM

data, where the complexity of the TME presents distinct analytical challenges. This manuscript builds on our foundational work but represents a significant advancement by adapting the pipeline specifically for IVM datasets.

While significant efforts have been made to develop open-source segmentation and tracking tools for live imaging data, including IVM[22–27] fewer tools exist for the unbiased analysis of tumor dynamics. One major barrier is that implementing such analytical methods often requires substantial computational expertise, limiting accessibility for many biomedical researchers conducting IVM experiments. To bridge this gap, we present BEHAV3D Tumor Profiler (BEHAV3D-TP) by providing a robust, user-friendly tool that allows researchers to extract meaningful insights from dynamic cellular behaviors without requiring advanced programming skills. BEHAV3D-TP expands the capabilities of BEHAV3D by incorporating key features designed for *in vivo* tumor cell dynamics (Fig. 1). The pipeline includes extensions that integrate tumor cell behavior with spatial features within the native TME, using either in situ (IVM) or fixed correlative imaging to reveal how distinct spatial niches influence tumor dynamics.

To further facilitate unbiased analysis of tumor dynamics, we developed BEHAV3D-TP as a flexible tool that supports both commercial and open-source data formats, ensuring broad compatibility across different research workflows. The pipeline supports 2D and 3D data formats generated by Imaris and by Fiji plugins such as TrackMate, MTrackJ, and ManualTracking, enabling processing of datasets from the most widely used segmentation and tracking solutions. We demonstrate the versatility and broad applicability of BEHAV3D-TP by applying it to a range of published tumor and healthy tissue IVM datasets.

Next, we focused on Diffuse Midline Glioma (DMG), a highly aggressive pediatric brain tumor characterized by invasive growth and its capacity to spread to other regions of the brain and the spinal cord [28]. Our approach allowed us to observe associations between DMG cell migration behavior and specific microenvironmental factors, including tumor-associated macrophages and vasculature, by visualizing TME components either during or after IVM. In our study, we specifically focused on cancer cell migration as a specific feature of DMG, but our methodology could easily be extended to other cancer cell behaviors such as intravasation or metastatic colonization. Overall, BEHAV3D-TP provides an accessible computational approach for a better understanding of tumor-TME crosstalk and the functional implications of this communication in heterogeneous tumors.

RESULTS

BEHAV3D Tumor Profiler: an accessible tool for mapping heterogeneity in tumor dynamics

To comprehensively map and analyze the dynamic heterogeneity of tumor cells within their TME we developed BEHAV3D-TP [https://github.com/imAIgene-Dream3D/BEHAV3D_Tumor_Profiler]. To enhance accessibility and encourage widespread adoption among researchers studying single tumor cell dynamics in live imaging and inspired by previous work on democratizing advanced image analysis[26,29,30], we designed BEHAV3D-TP as a modular Jupyter Notebook featuring an intuitive graphical user interface (GUI) (Figure 1 and Supplementary Video 1). The platform runs directly in a web browser and requires only a Google account for access. BEHAV3D-TP implementation within the Google Colaboratory (Colab) framework not only ensures efficient cloud-based computation with free and scalable resources but also enhances tool accessibility by eliminating the need for local software installation, a common barrier for inexperienced users. Regardless of programming proficiency, users can navigate the computational pipeline to extract comprehensive insights into tumor dynamics (Figure 1). After time-lapse image file processing and preparation using various frameworks (Figure 1a), the central component of BEHAV3D-TP — called the *heterogeneity module* (Figure 1b) — enables researchers to uncover diverse patterns of tumor morphodynamic behavior. Additionally, we provide two extension modules—the *large-scale phenotyping module* (Figure 1c) and the *small-scale phenotyping module* (Figure 1d)— which integrate tumor cell behavior identified with the *heterogeneity module* with TME features based on different data types. The *large-scale phenotyping* module uses post-IVM fixed imaging data for tissue phenotyping, identifying extensive regions with specific TME characteristics, and assessing the distribution of distinct tumor cell behavioral patterns within these regions. The *small-scale phenotyping* module uses *in situ*-labelled TME structures from IVM data, facilitating the correlation of these TME features within the microenvironment of individual tumor cell neighborhoods. Both modules, in conjunction with the *heterogeneity* module, help to identify how different aspects of the TME influence distinct behavioral patterns of tumor cells.

To evaluate the capability of the BEHAV3D-TP *heterogeneity module* in identifying diverse morphodynamic cell patterns, we applied it to IVM datasets from various tumor and healthy models. The datasets, processed with different segmentation and tracking tools, were analyzed

144 for multivariate similarities in morphological and dynamic features (summarized in Table 1)
145 using the dynamic time warping algorithm[21].

146 As an initial benchmark, we analyzed a previously published IVM dataset of two migratory and
147 metastatic breast cancer cell lines (4T1 and MDA-MB231), tracked in 2D using the MTrackJ
148 Fiji plugin (Supplementary Figure 1a) [15]. BEHAV3D-TP provided a more granular
149 characterization of these behaviors, uncovering additional migratory patterns not reported in
150 the original study (Supplementary Figure 1b-c). Specifically, we identified behaviors such as
151 *Fast*, *Intermediate*, *Very slow* and *Static* that had a different distribution among both tumor cell
152 lines (Supplementary Figure 1d-e).

153 To further assess the versatility of BEHAV3D-TP, we applied it to 2D IVM data of terminal
154 end buds (TEB) from healthy mammary gland tissue[31]. This dataset features confetti-labeled
155 epithelial cell types and was analyzed using maximum intensity projections of multiple z planes
156 showing cell morphology changes. As described in the original publication[31] cell segmentation
157 was performed with Cellpose 2.0[32] within the MaSCOT-AI workflow, followed by tracking
158 using the TrackMate plugin in Fiji. This workflow not only confirmed the compatibility of
159 BEHAV3D-TP with advanced segmentation frameworks but also its usage to unravel distinct
160 morphodynamic patterns in non-tumor epithelial cells (Supplementary Figure 2b,c). Consistent
161 with previous findings that HR+ TEB (Pr-cre/Confetti) exhibit greater migratory capacity than
162 HR- TEB (Elf5-rtTA/TetO-Cre/Confetti), our analysis suggests that this difference is primarily
163 driven by a distinct morphodynamic behavior (Supplementary Figure 2 c,d). Specifically, HR+
164 TEB more frequently exhibited characteristics of Cluster 2, defined by a rounder shape and
165 increased motility. Despite the small sample size requiring further validation, these results
166 demonstrate BEHAV3D-TP's ability to uncover complex, multiparametric cellular behaviors
167 that are often missed in analyses focused on single-value comparisons across conditions.

168 We next tested BEHAV3D-TP with a 3D image processing pipeline applied to IVM data from
169 adult glioma (GBM) [7]. In this case, cells were segmented using µSAM[33], a deep-learning
170 foundation model adapted for microscopy data (Segment Anything for Microscopy), and
171 subsequently tracked with TrackMate[27] Fiji plugin (Supplementary Figure 3a). BEHAV3D-TP
172 identified distinct GBM morphodynamic patterns, each characterized by unique combinations
173 of morphological and dynamic features and associated with specific spatial distributions
174 (Supplementary Figure 3b-d). Cluster 1, consisting of large and slow-moving cells, was more
175 isolated and located farther from neighboring cells compared to Cluster 6 (small, fast, persistent

176 cells) and Cluster 4 (very small, static cells). These findings suggest that the compact spatial
177 arrangement of small cells within the tumor may contribute to their reduced size.

178 Collectively, these findings underscore the versatility and broad applicability of BEHAV3D-
179 TP across diverse biological systems, dimensionalities (2D and 3D), imaging modalities, and
180 data processing pipelines, supporting its utility as a robust tool for the in-depth analysis of
181 cellular behavioral patterns in IVM data.

182 **Identification of highly heterogeneous *in vivo* cell behavior displayed by DMGs**

183 We then applied our platform to get insights into the behavioral heterogeneity among pediatric
184 DMG tumors, characterized by a highly invasive nature. We implanted mice with patient
185 derived DMG cells expressing H2BmNeonGreen marker and performed IVM for up to 5.4
186 hours upon tumor development (Figure supplement 4a). We tracked intravitally imaged DMG
187 cells from different mice using Imaris, a commercial software a widely adapted by the IVM
188 community[34–40] for its intuitive 3D visualization and analysis capabilities. In each imaged
189 position, we evaluated not only the dynamic characteristics of individual DMG cells but also
190 their spatial relationship to the tumor edge, which was delineated using Imaris Surface module
191 (Figure 2a, see Methods). Next, to untangle the complexity of tumor cell dynamics in an
192 unbiased manner, we used the BEHAV3D-TP *heterogeneity module,* implementing
193 multiparametric single-cell time-series classification to identify distinct single-cell behavioral
194 patterns (Figure 2 a, b). For this, we used kinetic parameters, including displacement, speed,
195 persistence, and movement direction relative to the tumor edge (Table 1), followed by
196 dimensionality reduction to classify cells. The BEHAV3D-TP *heterogeneity module* identified
197 7 DMG behavioral clusters: *retreating*, *slow retreating*, *erratic*, *static*, *slow*, *slow invading,* and
198 *invading* (Figure 2b, c, d, Supplementary video 2). To accurately describe each of the clusters,
199 we analyzed their most predominant features (Figure 2d) and back-projected the cluster
200 information into the original time-lapse to visually inspect cell behavior in relation to the tumor
201 (Figure 2a, c, Figure supplement 4b, Supplementary video 2). Of particular interest were cells
202 from the *invading* and *retreating* clusters, characterized by fast movement away from and
203 towards the tumor edge, respectively (Figure 2c-f, and Figure supplement 4c). In fact, in this
204 particular DMG model, approximately 10% of the cancer cells were displaying *invasive*
205 behavior (Figure supplement 4d), in line with the intrinsic infiltrative nature of DMG[41] .
206 Interestingly, about another 10% of DMG cells were moving back to the tumor edge (*retreating*,
207 *slow retreating* clusters) (Figure supplement 4d), behavior that has been previously observed
208 for glioblastoma and suggested to be regulated by differential chemotactic signaling by the

209 tumor edge and the surrounding brain parenchyma[7]. We also observed *erratic* cells that display
210 fast non-directed migration behavior, and *static* cells that are non-migratory (Figure 2c-f).
211 Crucially, the distinct behavioral patterns were detected in all intravitally imaged mice (Figure
212 supplement 4d), ruling out any sample bias that might lead to clusters consisting solely of cells
213 from a single tumor or mouse. This underscores the effectiveness of the BEHAV3D-TP in
214 revealing representative heterogeneous tumor behavioral patterns.

215 Mapping *in vivo* tumor cell migratory properties to distinct TME regions identified 216 through *ex vivo* large-scale 3D imaging

217 To investigate whether the TME influences behavioral heterogeneity among cancer cells, we
218 developed two complementary approaches to correlate the identified behavioral clusters (Figure
219 2) to the composition of the TME (Figures 1c, 3a and 4a).

220 The first approach consists of performing large-scale TME phenotyping and identifying regions
221 with a specific cellular composition and architecture within the TME of intravitally imaged
222 tumors that were subsequently fixed. This is accomplished by using multispectral large-scale
223 single-cell resolution 3D (mLSR-3D) imaging data[42,43] and a spatial analysis framework called
224 CytoMAP[44] (Figure 3a). We selected microenvironmental components of interest, such as
225 perivascular niches and glial cells, as they have been previously reported to play an important
226 role in the invasive behavior of glioblastoma cells[7,45–49]. Specifically, intravitally imaged brains
227 were collected immediately after the IVM imaging sessions and were fixed and stained for
228 blood vessels (CD31), oligodendrocytes (Olig2), and tumor-associated microglia/macrophages
229 (TAMM) (Iba1) (Figure 3b). Subsequent CytoMAP[44] spatial phenotyping analysis identified
230 three different environmental niches: *Void* regions (less vascularized and with low glial
231 infiltration), *TAMM/oligo* regions (enriched in oligodendrocytes, TAMM, and tumor cells), and
232 *TAMM/vascularized* regions (highly vascularized regions enriched in TAMM) (Figure 3b, and
233 Figure supplement 5a-c). To investigate the heterogeneity of tumor cell behavior in relation to
234 the identified microenvironmental niches, BEHAV3D-TP *large-scale phenotyping module*
235 mapped the different niches (*Void*, *TAMM/Oligo*, and *TAMM/vascularized*) identified by
236 CytoMAP onto 3D intravital imaging data (Figures 1c, 3c). In the TME-defined IVM-imaged
237 positions we compared the frequencies of the different behavioral clusters that we identified
238 with the BEHAV3D-TP *heterogeneity* module (Figure 3d). Interestingly, *invading* cells were
239 more abundant in *TAMM/vascularized* regions compared to *Void* regions that contain a higher
240 proportion of *static* cells, and *TAMM/Oligo* microenvironments contain more *slow retreating*
241 cells compared to the other regions (Figure 3d, Figure supplement 5d). Finally, we compared

242 the results obtained with BEHAV3D-TP to a more classical IVM analysis approach that relies
243 on assessing single dynamic parameters. Interestingly, single parameters showed a restricted
244 ability to identify differences in cellular behavior among various environments (Figure
245 supplement 5e-g), underscoring the importance of multiparametric behavioral mapping in
246 revealing more nuanced cellular behavior that cannot be captured solely by individual dynamic
247 parameters.

248 **Linkage of *in vivo* tumor cell behavior to the composition of the microenvironment at a**
249 **single-cell level**

250 With the goal of further refining TME phenotyping to better understand tumor cell behavior
251 determinants, we implemented an alternative approach using the BEHAV3D-TP *small-scale*
252 *phenotyping module* (Figure 1d, 4a). This module utilizes the detection of TME components
253 during IVM to offer insights into their abundance and spatial relationship with DMG cells at a
254 single-cell level. Together with the *heterogeneity module* that profiles the single-cell behavior
255 of tumor cells (Figure 1), this additional module allows linking different DMG behavioral
256 profiles with DMG cell small-scale niches (Figures 1d, 4a). For *in vivo* TME labeling, we
257 injected mice with an anti-CD31-AF647 antibody to label blood vessels, and with either SR101,
258 a fluorescent marker known to label oligodendrocytes and astrocytes [50–53], or CD20r, a novel
259 molecule described to label microglial cells [54] (Figure supplement 6a, b). This allowed us to
260 measure spatial TME characteristics of each single DMG cell, such as minimal distance to a
261 certain TME component, the number of these cell types in a certain radius, or the cell density
262 for this particular cell (Figure 1d). Interestingly, the BEHAV3D-TP *small-scale phenotyping*
263 *module* revealed substantial TME heterogeneity across the different behavioral DMG clusters
264 (Figure 4b). Compared to *slow* and *slow-retreating* cells, *invading* cells were usually found to
265 be less densely positioned relative to other DMG cells (Figure 4b, and Figure supplement 6c),
266 correlating with their invasive potential into the brain parenchyma. In line with the data from
267 the large-scale TME phenotyping (Figure 3), our data suggests that *invading* DMG cells reside
268 in a local environment that is enriched in TAMMs (Figure 4b). Indeed, *invading* cells are closer
269 to TAMMs compared to *erratic* and *slow* migrating cells (Figure 4c), and move directionally
270 towards TAMMs (Figure 4d, Supplementary video 3), suggesting that migration of this
271 behavioral cluster is at least partially mediated by chemotaxis. Furthermore, all fast-migrating
272 behavioral clusters (*invading*, *erratic,* and *retreating*) were found to be generally closer to blood
273 vessels (Figure 4b and e), suggesting that perivascular invasion is a more efficient movement
274 route for these cells (Figure 4f), a mode of migration that has been previously observed for adult

glioblastoma cells as well [7,45,47–49]. Lastly, particularly *slow-retreating* DMG cells were found in regions enriched for SR101^{+} cells (Figure 4b and Figure supplement 6d), perhaps reflecting oligodendrocyte-like (OC-like) tumor DMG cells that have been found near oligodendrocytes [55]. Altogether, these data demonstrate the power of our BEHAV3D-TP pipeline in correlating single-cell tumor cell behavior to its local environment, with an important opportunity to identify novel environmental regulators of invasion.

DISCUSSION

Here, we provide a new user-friendly platform tailored for IVM single tumor cell dynamics analysis, termed BEHAV3D-TP, aiming to better understand the mechanisms underlying tumor heterogeneity. In contrast to traditional pipelines that rely on the analysis of single parameters such as cell speed or displacement[56–58] or that use an artificial threshold to assign a specific behavior to cells[10], BEHAV3D-TP is an unbiased approach based on the integration of multiple parameters measured by IVM. Using the *heterogeneity module* of our BEHAV3D-TP pipeline, we uncovered behavioral phenotypes that have not been described before and that could not have been identified using single parameter analysis. For example, our analysis revealed *invading* and *retreating* clusters, composed of cells with a similar cell speed but with an opposite migration direction, an important biological and clinical difference. Likely, bidirectional migration is mediated by different chemotactic cues and by the composition of the local TME[59]. It is of vital importance for DMG and other cancer patients to better understand the biology underlying the different behavioral phenotypes, especially concerning *invading* cells that are difficult to therapeutically target [60].

Previous studies suggest a major role for the microenvironment in promoting tumor cell spread into the healthy brain [61–63]. Indeed, using the complementary *large-* and *small-scale TME phenotyping modules* of BEHAV3D-TP, we identified substantial differences in the TME composition of the different behavioral DMG clusters. Our results also show that the small-scale TME analysis has a higher predictive value compared to the large-scale TME analysis, suggesting that a cell's direct microenvironment is a more important regulator of its behavior compared to its macroenvironment. Future experiments directed towards identifying more TME components, for example using multispectral LSR-3D imaging[42], could therefore further refine the *large-scale phenotyping module* by detecting subregion heterogeneity.

IVM enables simultaneous labeling of various TME components and allows real-time investigation of their association with tumor cell behavior. Indeed, we found that TAMMs and

307 blood vessels were associated with specific behavioral phenotypes, showing the power of
308 BEHAV3D-TP *small-scale phenotyping module* in identifying novel regulators of cellular
309 behavior. This is exemplified by our finding that *slow-retreating* DMG cells were found in
310 environments enriched for $SR101^{+}$ cells, an observation that has not been made before. To take
311 further advantage of BEHAV3D-TP, future work should be directed toward identifying more
312 TME components, including cells of the adaptive immune system. For example, it would be
313 interesting to use our pipeline on recently developed immunocompetent mouse models of
314 DMG[64,65], or in mice with a humanized immune system[66]. While our findings suggest that
315 microenvironmental factors may influence tumor cell migration, further studies will be
316 necessary to establish causal relationships. Additional experimental validation, such as
317 macrophage ablation experiments, could help clarify the specific contributions of these factors.

318 While our current study does not provide direct functional validation of the distinct motility
319 clusters identified, existing literature strongly supports the notion that cell dynamics can serve
320 as a proxy for functional states and phenotypic heterogeneity. Prior work, including studies by
321 our group[19,67] as well as Crainiciuc et al.[36] and Freckmann et al.[20], has demonstrated that
322 variations in cell motility patterns can reflect underlying functional characteristics. Specifically,
323 cell morpho-dynamic features have been shown to correlate with differences in cell type
324 identity, T-cell engagement, metastatic potential, and drug resistance states. This growing body
325 of evidence suggests that tumor cell behavior, as captured by BEHAV3D-TP, may serve as a
326 predictive tool for deciphering functional tumor heterogeneity. Future studies integrating
327 transcriptomic or proteomic profiling of motility-defined subpopulations could further elucidate
328 the biological significance of these behavioral phenotypes.

329 In addition to motility-based classification, features such as tumor cell morphology,
330 proliferation state, and interactions with the tumor microenvironment can further refine tumor
331 phenotyping. BEHAV3D-TP allows for the selection of diverse feature types, supporting
332 datasets that include both dynamic, morphological and spatial parameters. However, we
333 recognize that expanding the feature set may introduce biologically irrelevant noise, particularly
334 in 3D microscopy data where limited z-axis resolution can lead to morphological artifacts. This
335 highlights the potential need in the future to include unbiased feature selection strategies, such
336 as bootstrapping methods[68], to ensure the identification of meaningful and biologically relevant
337 parameters. Careful consideration of these aspects is key to maximizing the interpretability and
338 predictive value of analyses performed with BEHAV3D-TP.

To enhance the accessibility of BEHAV3D-TP for researchers keen on studying tumor cell behavioral profiles through live imaging, we have incorporated our software in a Google Colab notebook, allowing researchers with minimal programming skills to employ the tool online without the requirement to install specific software environments nor the need to directly interact with the code. The user can easily install the necessary dependencies, set up the working environment, process datasets and adjust parameters without requiring deep coding skills. Google Colab provides the necessary computational resources to be able to run the pipeline without demanding a powerful local machine. However, there are RAM usage and runtime limitations that could affect the analysis, given a big enough dataset in the free version of Google Colab. Given this and data privacy concerns, the workflow can also be run locally via a Jupyter Notebook, that can be downloaded from the Google Colab notebook. Aligned with the goals of BEHAV3D-TP, other methods utilizing the Google Colab framework are emerging, such as CellTracksColab[29], which is a general tool for tracking data analysis. While CellTracksColab offers valuable insights into tracking data, BEHAV3D-TP is specifically designed for IVM data and includes additional features. These features include directionality metrics crucial for invasion studies, detailed analysis of identified behavioral populations, data back-projection, and correlation of these behaviors with both large-scale and small-scale TME features. This comprehensive approach provides a deeper understanding of the TME drivers behind intratumoral heterogeneity, making BEHAV3D-TP a robust tool for researchers investigating the complex behaviors of tumor cells in their natural environments. BEHAV3D-TP supports a broad range of data formats, including those generated by commercial Imaris and by open-source Fiji plugins such as TrackMate, MTrackJ, and ManualTracking, increasing the tool's applicability to researchers using both commercial and open-source pipelines.

In summary, BEHAV3D-TP allows to get insights into the heterogeneity of tumor cell migration behavior in an accessible way; however, it would be exciting to extend the application to other behaviors, such as cell division or therapy response to study TME-mediated drug resistance.

366 **METHODS**

367 **Animal material**

368 NOD.Cg-PrkdcscidIl2rgtm1Wjl/SzJ (NSG) mice were purchased from Charles River
369 Laboratories (France). Experiments were conducted per Institutional Guidelines under acquired
370 permission from the local Ethical Committee and as per current Dutch laws on Animal
371 Experimentation. Mice were housed under sterile conditions using an individually ventilated
372 cage (IVC) system and were fed with sterile food and water.

373 **Human DMG sphere-forming culture**

374 DMG007 (HSJD-DIPG-007) cells established from primary DMG material were grown in a
375 base medium (TSM) consisting of 48% DMEM/F12 and 48% Neurobasal medium (Thermo
376 Fisher) supplemented with GlutaMAX, 100mM Sodium Pyruvate, MEM non-essential amino
377 acids and 1M Hepes buffer, at 1% each. Primocin (InvivoGen) at 50mg/ml was additionally
378 added to the TSM. Working medium was prepared by adding 20ng/ml of human EGF and
379 human basic FGF, 10ng/ml of PDGF-AA and PDGF-BB (Peprotech) and 2ug/ml of Heparin
380 (StemCell Technologies). DMG cells were cultured at 37 °C in a humidified atmosphere with
381 5% CO_2.

382 **Fluorescent reporter cloning and lentiviral transduction**

383 Fluorescent reporter construct was based on the combination of Histone2B-mNeonGreen, P2A
384 and mScarlet I-CAAX gifted from Dr. Hugo Snippert (UMC Utrecht, The Netherlands), and
385 inserted by In-Fusion HD Cloning Plus (Takarabio) into a lentiviral vector including
386 cPPT/CTS, WPRE, an EF1a promoter and IRES-puromycin-resistance cassette[11]. Subsequently
387 the above-mentioned elements were amplified by PCR and the amplicon was assembled in the
388 final lentiviral backbone using Gibson Assembly (NEB). Sequences were validated using
389 Sanger sequencing. DMG007 cells were transduced using a standard lentiviral transduction
390 protocol and selected using puromycin to achieve a stable cell line.

391 **Cranial imaging window (CIW) surgery and tumor cell injection**

392 CIW surgery and tumor cell injection were performed on the same day as previously described
393 [7,10]. Briefly, mice were sedated with Hypnorm (Fluanison [neuroleptic] + Fentanyl [opioid])
394 (0.4 ml/kg) + Midazolam [benzodiazepine sedative] (2 mg/kg) at a dose of 1:1:2 in sterile water
395 and mounted in a stereotactic frame. The head was secured using a nose clamp and two custom-
396 made 3D printed ear bars, made out of Polylactic Acid (PLA, Geeetech, 700-001-043). The

397 head was shaved, and the skin was cut circularly. The mouse was placed under a stereo-
398 microscope to ensure precise surgical manipulation. The periosteum was scraped, and a circular
399 groove of 5 mm diameter was drilled over the right parietal bone. The bone flap was lifted under
400 a drop of cortex buffer (125 mM NaCl, 5 mM KCl, 10 mM glucose, 10 mM HEPES buffer,
401 2 mM $MgSO_4$, and 2 mM $CaCl_2$, pH 7.4), and the dura mater was removed. Gelfoam sponge
402 (Pfizer) was used to stop potential bleedings. Next, 1×10^5 DMG007-H2B-mNeonGreen cells
403 resuspended in 3 µl phosphate-buffered saline (PBS) were injected stereotactically using a 5 µl
404 Hamilton syringe with a 2 pt style in the middle of the craniotomy at a depth of 0.5 mm. The
405 exposed brain was sealed with silicone oil and a 6 mm coverslip was glued on top. Dental
406 acrylic cement (Vertex) was applied on the skull surface, covering the edge of the coverslip,
407 and a custom-made 3D printed ring made of biocompatible Polylactide acid (PLA, Geeetech,
408 700-001-0433) was glued around the coverslip to provide fixation during intravital imaging and
409 to serve as a reservoir for a water drop required for the objective of the microscope. A single
410 dose of 100 µg/kg of buprenorphine (Temgesic, BD pharmaceutical limited) was administered
411 for post-surgical pain relief. Mice were closely monitored twice per week to assess behavior,
412 reactivity, and appearance.

413 **Intravital imaging**

414 For DMG IVM imaging mice were intravitally imaged as previously described [7,10]. In short,
415 mice were sedated with isoflurane and placed face-down in a stereotactic frame. The Polylactide
416 ring was used to fix the mouse's head to the frame with custom-made Polylactide bars. Time-
417 lapse images of the entire tumor volume were acquired for a maximum of 5.4 hours. The
418 minimal time interval between serial images was set to 20 minutes. For tile scans, images of the
419 complete z-stack of the tumor were acquired, with a step size of 2 µm. In a group of 3 mice,
420 oligodendrocytes and astrocytes were imaged by an intravenous injection of 50 µL SR101
421 (Thermofisher) at a concentration of 5 mM dissolved in PBS. In a different group of 3 mice,
422 TAMMs were imaged by intravenous injection of 50 µL 100 µM CDr20[54]. Simultaneously with
423 the injection of either SR101 or CDr20, all mice received an intravenous injection of 10 ul
424 CD31-AF647 antibody (ThermoFisher, A14716) to visualize the blood vessels.

425 Intravital imaging was performed on an upright FVMPE-RS multiphoton microscope
426 (Olympus) equipped with a MaiTai DeepSee and an InSight DeepSee laser (Spectra-Physics),
427 a 25x/1.05 numerical aperture water objective, and two GaAsP and two Multialkali
428 photomultiplier tubes (Olympus). Images were acquired with simultaneous imaging with the
429 MaiTai (960 nm) and Insight (1100 nm) lasers. Green, red, and far-red fluorescence was

separated by 570 nm and 650 nm dichroic mirrors, and 610/70 nm and 705/90 nm filters (Semrock) and collected by GaAsP or Multialkali photomultiplier tubes. Scanning was performed in a bidirectional mode with a resonant scanner at 400 Hz and 12 bit, with a zoom of 1x, 512 × 512 pixels. For optimal detection of blood vessels (CD31-AF647), a single tile scan was made at the last timepoint with Insight laser tuned at 1250 nm. At the postprocessing step, this image was co-registered to the time-lapse movie.

Breast tumor IVM imaging was performed as described before[15] and data was kindly provided by Dr. Nienke Vrisekoop. GBM IVM imaging was performed as described before[7] and data was kindly provided by Prof. Jacco van Rheenen. Breast epithelial IVM imaging and cell tracking with MaSCOT-AI was performed as described before[31] and single cell tracks were downloaded from Zenodo repository (14503476).

Co-registration of IVM imaged blood vessel imaging

CD31-AF647 tile scan featuring optimal visualization of blood vessels during live imaging was co-registered to the last timepoint of the time-lapse movie. Both images (last timepoint of time-lapse tile-scan and blood vessel tile-scan) were visually inspected to determine and annotate the internal landmarks using Imaris (Oxford Instruments), versions 9.5 to 9.6. These landmarks served as a reference for the co-registration software to overlap both images. To perform the co-registration, a modification of *elastix*[69] was used; a python-based open-source software based on Insight Segmentation and Registration Toolkit (ITK) plus SimpleElastix[70] : a collection of different algorithms used on medical image registration. Due to the extensive number of potential parameter combinations, specific parameters were manually chosen. This selection was conducted using the Slicer3D visualization software, version 5.2.2.

Immunohistochemistry

3D immunohistochemistry was performed as described before [43]. After the live imaging session, mouse brains were immersed in 5 ml 4% paraformaldehyde (PFA) pH 7.4 overnight on ice. After fixation, brains were blocked in 5-10 ml Wash Buffer 1 (2 ml Tween-20, 2 ml Triton X-100, 2 ml 10% SDS, and 2 g BSA in 1 l PBS) for 5 hours. For multiplex immunolabeling, a two- or three-round staining protocol was used as previously described[42,43]. Washing and incubation steps were performed in Wash Buffer 2 (1 ml Triton X-100, 2 ml 10% SDS, and 2 g BSA in 1 l PBS). A thick (1 mm) slice of the cortex part that was under the cranial imaging window was dissected with a scalpel before proceeding to immunolabeling. The following primary antibodies were used: rabbit anti-Olig2 1:100 (AB9610, Merk), goat anti-Iba1 1:200

462 (NB100-1028SS, NovusBio) and CD31-AF647 1:250 (A14716, ThermoFisher). As secondary
463 antibodies, donkey anti-rabbit AF405 1:250 (ab175651, Abcam) and donkey anti-goat AF633
464 1:250 (A21082, ThermoFisher) were used. After the last washing step, tissues were optically
465 cleared by three stepwise incubations of an increasing concentration of FUnGI[71] clearing agent
466 (25%/50%/75%, diluted in PBS) for 1h at room temperature[42]. The final incubation step with
467 100% FUnGI was performed overnight at 4°C.

468 **mLSR3D imaging**

469 mLSR3D imaging[42,43] of thick slices of fixed mouse cortex was performed using a Zeiss
470 LSM880 system equipped with a 32-channel spectral detector. The signal from all fluorophores
471 present in the samples was collected in a single acquisition and linear unmixing was used to
472 obtain separate channels. Unmixing was carried out by the Online Fingerprinting mode of the
473 microscope. Pre-acquired references of each single fluorophore were used to enable
474 multispectral on-the-fly unmixing. Imaging was performed using a 25x multi-immersion
475 objective 0.8 NA (Zeiss 420852-9871) with a working distance of 570µm. Tile scans were
476 acquired using a voxel size of 0.332x0.332x1.200 µm, a pixel dwell of 2µs, and a 10% tile
477 overlap.

478 **Imaris image processing**

479 DMG IVM datasets were processed using Imaris software (Oxford Instruments, versions 9.5 to
480 10.1) for 3D visualization, shift correction, object rendering, and cell tracking of time-lapse
481 movies.

482 ***Imaris Cell tracking***

483 The *Channel Arithmetics* Xtension was used for channel unmixing of overlapping signals. The
484 Spots ImarisTrack module was used for object detection and semi-automated tracking of tumor
485 cells (autoregressive motion). Tumor cell tracks were manually corrected to ensure accurate
486 tracking. Around 50-100 cells per position were manually corrected and labeled as such for
487 posterior selection of accurate tracks. To determine the direction of tumor cell movement
488 relative to the tumor core, at the image edge closer to the tumor core a "Tumor edge" surface
489 object was manually rendered using the contour tool. The *Distance Transformation* Xtension
490 was used to measure the distance between tumor cells and the "Tumor edge". For tracked tumor
491 cells, time-lapse data containing the coordinates of each cell, the values of cell speed, mean
492 square displacement, displacement delta length, displacement length, and distance to "Tumor

493 edge" were exported. See https://qbi.uq.edu.au/files/40820/ImarisManual.pdf for statistical
494 details.

495 ***Imaris Microenvironmental factors rendering***

496 For rendering the microenvironmental factors detected during IVM or by post-IVM LSR-3D
497 imaging, the Surface and Spots modules of Imaris were used. Surfaces were used for the SR101,
498 CDr20, Olig2, DAPI, and Iba1 stainings, and Spots were used for CD31+ protruding or
499 elongated structures, as previously described [44]. For rendered structures, positional data
500 containing the coordinates of objects were exported for large-scale spatial phenotyping with
501 Cytomap.

502 **Fiji image processing**

503 ***µSAM cell segmentation***

504 Segmentation was performed using the µSAM plugin for Napari[33] , where *vit-b* model was
505 selected to compute embeddings for each timeframe. Automatic segmentation was applied, and
506 parameters were adjusted for optimal results. Manual corrections were made to remove
507 unwanted surfaces or add missing cells. Once segmentation was complete, frames were
508 combined into a single stack in ImageJ and tracked with Trackmate.

509 ***Fiji tracking***

510 Breast tumor IVM data was manually tracked with Fiji MtrackJ plugin as previously
511 described[10,15] .

512 Adult glioma cells, segmented with µSAM, were consequently tracked with Fiji TrackMate
513 plugin. The labeled image stack, segmented using µSAM, was imported into ImageJ for cell
514 tracking with the Fiji TrackMate plugin. The "Label Image Detector" was employed to identify
515 individual cells, and the LAP Tracker was used to link cells across timeframes. Tracking
516 parameters were optimized to account for missing frames and ensure accurate cell trajectories.
517 The statistics for each tracked cell were subsequently exported. To integrate both dynamic and
518 morphological data, a custom script was developed to merge the dynamic information from
519 TrackMate with the morphological data obtained from the µSAM segmentation labels for each
520 individual cell. This integration was achieved by assigning the "TRACK_ID" from the
521 TrackMate "allspots" output file to each segmented instance extracted from the TIFF file. The
522 assignment was performed using the "measure" function in scikit-image and the KDTree
523 distance function from the scipy module, based on the x, y, and z positions of the cells.

The script is available both as a downloadable version on GitHub (https://github.com/imAIgene-Dream3D/MorphoTrack-merger) and as an online application (https://morphotrack-merger.streamlit.app/), making this tool more accessible for non-coding users.

Tumor large-scale spatial phenotyping with Cytomap

The positional data of various environmental surface features, segmented from LSR-3D imaging data, was analyzed for large-scale spatial phenotyping using the Cytomap Spatial Analysis Toolbox[44]. Briefly, neighborhoods with a 100 µm radius were generated. Neighborhoods were then clustered into 2 regions based on DMG cell positioning using the David Balwin algorithm. Using the gating tool, the tumor regions (containing DMG objects) were defined. Next, the neighborhoods were clustered again into 3 different regions based on the distribution of Iba1, Olig2, and CD31: *Void, TAMM/Oligo,* and *TAMM/vascularized*. By using the *Manually Defined Regions* option, only the tumor region was classified. Finally, for each region, fold-change values were calculated and exported using the *Region Statistics* tab. To map the assigned regions onto IVM movies, a 3D image of the cluster distribution within the tumor was generated and exported for each sample (Figure Supplement 5a). Next, regions within the IVM movies were visually matched to the corresponding regions identified by the Large-Scale Phenotyping module of Cytomap (Figure 3c). For each mouse, at least one or two representative positions per matched region type were selected, cropped, and analyzed to assess tumor cell behavior, following the previously described cell tracking methodology (*Imaris Cell tracking*).

BEHAV3D Tumor Profiler framework

BEHAV3D-TP was developed using the R Studio version 4.3.3. It features three modules: 1) *Heterogeneity module* with optional 2) *Large-scale and/or* 3) *Small-scale phenotyping module.* These modules are described in detail below, exemplified by the analysis of DMG data from this study. All of the modules are included in the same script available in Github [https://github.com/imAIgene-Dream3D/BEHAV3D_Tumor_Profiler], but can be run independently from one another. To acquire this independency, the optional modules are directly combined to the necessary sections of the *Heterogeneity module*. Consequently, the user can use whichever module is best suited for their purposes. The complete workflow—combining heterogeneity analysis with large- and small-scale phenotyping—is primarily optimized for datasets processed with Imaris due to its wide use in the IVM community and

special suitability for 3D visualization and tracking. In order to further facilitate public access to the BEHAV3D-TP, a Google Colab notebook has also been created accessible through the same Github page [https://github.com/imAIgene-Dream3D/BEHAV3D_Tumor_Profiler]. This environment is friendly to anyone regardless of their coding expertise as it has a step-by-step follow-through execution through the pipeline.

In addition, to broaden accessibility and support alternative data processing pipelines, the core *Heterogeneity module* of BEHAV3D-TP is also compatible with Fiji-based tracking data, specifically outputs generated by TrackMate. MTrackJ and ManualTracking. A separate Google Colab notebook is provided for these workflows on the Github page, allowing users to easily import Fiji-processed datasets, adjust analysis parameters, identify different morpho-dynamic single cell patterns.

A Wiki demo run and a video tutorial (Supplementary Video 1) are also provided through the GitHub page [https://github.com/imAIgene-Dream3D/BEHAV3D_Tumor_Profiler] for further clarification.

To ensure that your input data aligns with the workflow, we provide an online application for data quality control (https://github.com/alievakrash/BEHAV3D_TP_dataQC). This tool allows users to visualize various features, grouped by a condition of interest, and check for issues such as a high number of missing values (NA). It enables users to assess their data for any inconsistencies or unexpected patterns before proceeding with further analysis.

Heterogeneity module.

To account for missing time points and to create a time series with the same time interval for each tumor cell time series, linear interpolation was used to estimate the values of missing time points. To compare time series independently, tracks were cropped to the minimal common length among all tracks. In the case of DMG data to a 2.6 hour duration. For tracked tumor cells, time-lapse data containing the coordinates of each cell, the values of cell speed, mean square displacement, displacement delta length, displacement length, and relative distance to "Tumor edge" were used to calculate a cross-distance matrix between time series. First, we performed a principal component (PC) analysis and selected the number of PCs that explained at least 90% of data variance (3).

The previously calculated PCs were then used to compute the cross-distance matrix between each tumor cell multivariate time series using the dynamic time warping algorithm from the

package “dtwclust”. To visualize heterogenous tumor cell behaviors in 2 dimensions, dimensionality reduction on the cross-distance matrix was performed by the Uniform Manifold Approximation and Projection method (“umap” package). Clustering was performed using the k-means clustering algorithm. For each cluster, the average values of distinct behavioral and environmental components were calculated and plotted as a heatmap (“pheatmap”).

Large-scale phenotyping module.

The information obtained from mLSR3D and Cytomap about large-scale TME regions were combined with the DMG cells behavioral information (see above section *Tumor large-scale spatial phenotyping with Cytomap)* to examine the large-scale features of tumor cells. For tumor cells, the mean speed, square displacement and raw movement were analyzed.

Small-scale phenotyping module.

The positional coordinates of tracked tumor cells and detected microenvironmental factors were used to determine the small-scale landscape of tumor cells. For tumor cells, the average distance to the closest 10 neighbors was measured to determine tumor cell density. For each tumor cell and each environmental component, the number of microenvironmental objects in a 30-µm radius and the distance to the closest object were computed. For each behavioral cluster, the values of closest neighbors, minimal distance to each environmental factor, and number of environmental objects in the 30 µm radius were plotted and compared.

Statistical analyses

Statistical analyses were performed using R. The representation of *n* may refer to individual mice, distinct imaging positions within different mice, or individual cell tracks, as indicated in the figure legends. Two-tailed unpaired t-tests were performed for comparison between two groups unless indicated otherwise (Figure supplement 1d). For comparisons of more than two groups we performed a one-way ANOVA (Figure 2d and Figure 4b) followed by Tukey HSD correction (Figure Supplement 4c (p values in legend), Figure 3d, Figure 4 c,e, Figure Supplement b, e-g, Figure Supplement 6 c,d). To compare the distribution of different morphodynamic clusters of TEB cells, we pooled all positions and mice due to the low number of cells per position. We then constructed a contingency table and performed a Chi-square test (Figure supplement 2d). To compare the distance to the nearest neighbors between morphodynamic clusters of GBM cells, a mixed-effects linear regression was performed with mouse as a random effect (Figure supplement 3d).

Data availability

DMG imaging data is publicly available at BioStudies accession number S-BIAD1759 (https://www.ebi.ac.uk/biostudies/studies/S-BIAD1759). Breast cancer IVM data was previously described[15] and kindly provided by Dr Nienke Vrisekoop. Adult glioma IVM data was previously described[7] and kindly provided by Prof. Jacco van Rhennen. Healthy breast epithelium IVM was previously described[31] and kindly provided by Prof. Jane Visvader. Demo outputs and Jupyter notebooks of Imaris- and Fiji-processed data are provided in our GitHib repository (https://github.com/imAIgene-Dream3D/BEHAV3D_Tumor_Profiler).

Code availability

We provide the BEHAV3D-TP framework in a Google Colab user-friendly environment [https://colab.research.google.com/drive/1JI7ysqFf3tvdi6Df4YUsSZ8RbuXw8wba?usp=sharing], as well as in an R script format in Github [https://github.com/imAIgene-Dream3D/BEHAV3D_Tumor_Profiler]. Additionally, a Wiki [https://github.com/imAIgene-Dream3D/BEHAV3D_Tumor_Profiler/wiki] to follow through a demo dataset as well as a video tutorial (Supplementary Video 1) has been developed for further assistance. For the BEHAV3D-TP heterogeneity module, we offer an online app to assess data quality (https://behav3d-tp-data-qc.streamlit.app/), with the corresponding code available on GitHub (https://github.com/alievakrash/BEHAV3D_TP_dataQC). Additionally, for quantifying morphological features derived from Microsam segmentation and integrating them with dynamic features from TrackMate, we provide another online app (https://morphotrack-merger.streamlit.app/) and related code on GitHub (https://github.com/imAIgene-Dream3D/MorphoTrack-merger).

Acknowledgements

We thank the Princess Máxima Center for Pediatric Oncology for technical support and the Hubrecht Institute, Zeiss and the Princess Maxima Imaging Center for imaging support and collaboration. We thank D. van Vuurden (Princess Máxima Center for Pediatric Oncology) and Dr. Ángel Montero Carcaboso (Sant Joan de Déu Barcelona Hospital) for providing primary DMG cultures; Dr Young-Tae Chang (Postech, Korea) for providing us the CD20r dye; Dr Nienke Vrisekoop for sharing breast cancer IVM data; Prof. Jacco van Rheenen and Wouter Beijk for sharing adult glioma IVM data; Prof Jane Visvader for sharing breast epithelial IVM data; Dr Colinda Scheele and Marcel Issler for sharing healthy breast IVM data (explored but

not used in the current study); and members of the Dream3DLAB (Rios group) and imAIgene-lab (Alieva group) for offering critical feedback on the project. A.Z. was supported by a Veni fellowship from the Netherlands Organization for Scientific Research (09150161910076). R.C. and A.C.R were supported by an ERC-starting grant 2018 project (no. 804412). This work was produced with the support of a 2023 Leonardo Grant for Scientific Research and Cultural Creation, BBVA Foundation (LEO23-2-10305-BBM-BAS-144) and the V FERO-ASEICA Research Award (BFERO2024.04). M.A was supported by the Comunidad de Madrid (2022-T1/BMD-24021).

FIGURE LEGENDS

Fig. 1: BEHAV3D Tumor Profiler pipeline. Schematic representation of the workflow showing data preparation, input and outputs in each of the three modules. **a,** Time-lapse image processing and preparation, based on segmentation and tracking of tumor (and labelled TME cells). Mounting Google Drive is optional but recommended to work in the Google Colab framework. **b,** Heterogeneity Module provides distinct behavioral clusters for cells, and relates them to dynamic features and provides a back-projection of the tracked cells. **c, d,** Optional modules, additional to the Heterogeneity module. **c,** Large-scale phenotyping module combines TME large-scale information with cell morphodynamic profiling to further depict population frequencies in distinct TME regions. **d,** Small-scale phenotyping module combines TME small-scale information with morphodynamic profiling to depict how the cellular environment can influence tumor cell behavior.

Fig. 2: Behavioral profiling of DMG cells with BEHAV3D-TP heterogeneity module. a, Representative intravitally imaged position showing DMG cells tracked relative to tumor Edge (left panel). Tracks were classified according to DMG behavior (right, color coded by cluster). Representative of $n = 18$ independent positions from n=6 mice. **b,** UMAP plot showing seven color-coded DMG cell behavioral clusters identified by BEHAV3D-TP. Each datapoint represents one DMG cell track. A total of 981 individual cells were tracked in $n = 18$ independent positions from n=6 mice. **c,** Representative intravitally imaged positions and enlarged sections for showcasing distinct DMG behavioral clusters *Invading* (yellow), *Retreating* (green), *Erratic* (dark purple) and *Static* (light purple) through the time series. $n = 18$ independent positions from n=6 mice. Scale bars 10µm. **d,** Heatmap depicting relative values of DMG cell features indicated for each cluster, named according to their most distinct characteristics. Arbitrary units in respect to maximal and minimal values for each feature. See Table 1 for features description. Bubble size according to significance levels, all features

683 represented have a significance level of P < 0.001 (***): *mean_displ2, mean squared*
684 *displacement; speed; delta displacement; displacement length; persistence; invasion*. P-values
685 represent the significance of differences across clusters tested through ANOVA for each
686 feature. **e, f,** UMAP representation of DMG cells' velocity relative to the tumor edge(µm) (**e**)
687 and speed (µm/h) (**f**). Each datapoint represents one cell track and is colored following a color
688 gradient. For each feature colors represent the mean DMG track values. Representative
689 of $n = 18$ independent positions from n=6 mice.

690 **Fig. 3: Mapping distinct DMG behavioral patterns to distinct TME regions. a,** Overview
691 of the large-scale TME region phenotyping workflow. After IVM imaging session, the tissue is
692 fixed and stained and then analyzed using mLSR-3D. CytoMAP Spatial Analysis Toolbox is
693 used to identify distinct large-scale regions, that are subsequently matched to IVM imaging
694 dataset (c). **b,** Representative fixed multispectral image of a mLSR3D imaged DMG tumor and
695 zoomed-in images of TME large-scale regions: *Void* (blue outline), *TAMM/vascularized* (red
696 outline) and *TAMM/Oligo* (yellow outline). DMG nuclei (blue), CD31 (pink), Olig2 (purple),
697 and Iba1 (yellow) are represented on the imaged. Scale bars, 100 µm (overview), 30 µm
698 (zoomed-in regions). **c,** 3D multispectral image DMG cell rendering color-coded per large TME
699 region: *Void* (blue), *TAMM/Oligo* (yellow) and *TAMM/vascularized* (red) (left). Based on the
700 spatial coordinates of DMG cells classified into specific TME regions by CytoMAP, cells
701 within the mLSR-3D images were subsequently assigned to their respective TME regions.
702 Regions were then visually mapped on intravital imaging data (right). Representative of n=6
703 mice. White outline indicates one of the tumor regions analyzed with BEHAV3D-TP from the
704 full tumor volume. **d** Boxplots showing the frequencies of different DMG behavioral clusters
705 in *Void, TAMM/Oligo and TAMM/vascularized* TME large-scale regions. For each behavioral
706 cluster, the y-axis displays the z-scored percentage of cells, normalized per mouse to account
707 for inter-mouse variability. Each point represents an individual imaged position, with shape
708 indicating the mouse of origin. P-values represent the significance of differences across TME
709 regions tested through ANOVA with Tukey post hoc, for each behavioral cluster. $n = 18$
710 independent positions from n=6 mice.

711 **Fig. 4: The BEHAV3D-TP small-scale phenotyping correlates DMG behavioral profiles**
712 **with microenvironmental composition at a single-cell resolution. a,** Overview of the small-
713 scale TME phenotyping module. During IVM imaging, information about spatial distribution
714 of SR101+, CD20r+, and CD31+ cells is collected and processed by the BEHAV3D-TP *small-*
715 *scale phenotyping module*. Single DMG cell spatial TME features like distance to its neighbors,

716 number of cells in a radius or minimal distance to a cell type were measured. **b,** Heatmap
717 depicting DMG cell small-scale niches' features across distinct DMG behavioral clusters.
718 Arbitrary units in respect to maximal and minimal values for each feature. Bubble size
719 according to significance levels, from smallest (P < 0.05 (**)) to medium (P < 0.01 (**)) to
720 biggest (P < 0.001 (***)): *dist_10_cell*, Distance to nearest 10 cells, P < 0.01 (**); *n*_SR101,
721 number of SR101 cells, P < 0.05 (*); *min_SR101,* minimal distance to a SR101 cell, P < 0.05
722 (*); *n_CD20r,* number of CD20r cells, P < 0.05 (*); *min_Cd20r,* minimal distance to a CD20r
723 cell, P < 0.01 (**); *min_BV_dist,* minimal distance to a Blood vessel, P < 0.001 (***). P-values
724 represent the significance of differences across clusters tested through ANOVA for each
725 feature. **c, e,** Boxplot depicting the *Minimal distance to a CD20r+ TAMM (µm)* (**c**) and the
726 *Minimal distance to a blood vessel (µm)* (**e**) across DMG behavioral clusters. Each point
727 represents an individual tracked cell, color depicts the imaged position and shape denotes the
728 mouse. P-values represent the significance of differences across behavioral clusters tested
729 through ANOVA with Tukey's post hoc. P < 0.01 (**);P < 0.05 (*).P < 0.001 (***); P < 0.1
730 (·). **c**, $n = 10$ independent positions from $n=3$ mice. **e**, $n = 8$ independent positions from $n=3$
731 mice. **d,** Multispectral image showing the movement of DMG cells (grey) relative to CD20r+
732 TAMM (blue) and the Tumor core. The trajectories show a path from the initial (blue) to the
733 final position (red). Scale bar, 10 µm. **f,** Time lapse multispectral images (left to right) showing
734 the DMG cells (blue) displacement along CD31 blood vessel (purple) away from the tumor
735 edge. Scale bars, 30 µm.

736 **Figure supplement 1: Example application of BEHAV3D-TP for 2D movement pattern**
737 **analysis of breast cancer cells tracked with MTrackJ Fiji plugin. a)** Representative
738 intravitally imaged position showing breast tumor cells tracked in 2D with the MTrackJ plugin.
739 Red: MDA-MB-231 cells; Blue: Second Harmonic Generation; Multicolored tracks:
740 individually tracked cells. **b)** UMAP plot showing six color-coded breast tumor cell behavioral
741 clusters identified by BEHAV3D-TP. Each datapoint represents one cell track. A total of 935
742 individual cells were tracked. **c)** Heatmap depicting relative values of breast tumor cell dynamic
743 and spatial features indicated for each cluster, named according to their most distinct
744 characteristics. Arbitrary units in respect to maximal and minimal values for each feature. See
745 Table 1 for features description. **d)** Boxplots showing the percentages of different breast cancer
746 behavioral clusters for 4T1 and MDA-MB-231 cells. Each point represents a different imaging
747 position. P-values represent the significance between both conditions measured with a

Student's T test. **e)** Breast tumor cell tracks classified according to behavior (color coded by cluster in c). In all panels: representative of $n = 13$ independent positions from n=4 mice.

Figure supplement 2: Example application of BEHAV3D-TP for 2D morphodynamic analysis of cells segmented with CellPose2.0 and tracked using TrackMate.

a) Schematic overview of the segmentation and tracking pipeline using CellPose2.0 and TrackMate (see Methods). **b)** UMAP plot showing four color-coded morphodynamic clusters of healthy breast epithelial cells from TEBs identified by BEHAV3D-TP. Each datapoint represents one cell track. A total of 291 individual cells were tracked. **c)** Heatmap depicting relative values of epithelial cell dynamic and morphological features indicated for each cluster, named according to their most distinct characteristics. Arbitrary units in respect to maximal and minimal values for each feature. **d)** Stacked bar plot showing the distribution of morphodynamic cell types across the two indicated TEB populations: HR+ luminal progenitor cells and HR− luminal progenitor cells. Combined data from 19 mice and 72 independent positions. Chi-square test indicates p=0.02 for cluster 2.

Figure supplement 3: Example application of BEHAV3D-TP for 3D morphodynamic analysis of cells segmented with µSAM and tracked using TrackMate.

a) Schematic overview of the segmentation and tracking pipeline using µSAM and TrackMate. An online app was developed to integrate morphological and dynamic features (see Methods). **b)** UMAP plot showing four color-coded morphodynamic clusters of GBM cells identified by BEHAV3D-TP. Each datapoint represents one cell track. Total of 460 individually tracked cells. **c)** Heatmap depicting relative values of GBM cell dynamic and morphological features indicated for each cluster, named according to their most distinct characteristics. Arbitrary units in respect to maximal and minimal values for each feature. See Table 1 for features description. **d)** Boxplot showing *Average distance to the 3 closest GBM neighbors (pixels)* across distinct GBM morphodynamic clusters. Each point represents an individual tracked cell, with color indicating the imaged position (n = 6) and shape representing the mouse (n = 4). P-values denote statistical significance across behavioral clusters, assessed using a linear mixed model with mouse as a random effect, followed by Tukey's post hoc test. $P < 0.001$ (***).

Figure supplement 4: DMG cells heterogeneity captured by intravital imaging. a, Schematic representation of an intravital imaging experimental design, capturing timelapses up to 5.4 hours of DMG cells expressing H2BmNeonGreen and mScarlet proteins, followed by single-cell tracking. **b,** Representative intravitally imaged position showing DMG cell tracks

780 colored by behavioral cluster projected over the last timepoint of the original IVM time-lapse.
781 **c,** Quantification of average DMG cell speed (µm/h) in each identified behavioral cluster.
782 Significance of differences across behavioral clusters tested through ANOVA followed by
783 Tukey's post hoc test. All comparisons significant, except cluster 3-4 and 6-4. **d,** Behavioral
784 cluster frequency distribution across individual IVM imaged mice. Each point indicates an
785 individual cell track, color depicts *n* = 18 independent positions; shape depicts *n*=6 mice.

786 **Figure supplement 5: Cell type and behavioral cluster frequency distribution in identified**
787 **TME large-scale regions. a,** Representative CytoMap output showcasing**,** 3D spatial
788 distribution of DMG cells in distinct TME large-scale regions: *Void* (blue), *TAMM/Oligo*
789 (yellow) and *TAMM/vascularized* (red). Each datapoint represent a unique DMG cell within a
790 classified large-scale region. **b, c,** Fold change of cell count of DMG, Iba1+, Olig2+ and CD31+
791 cell types, identified with mLSR3D fixed imaging, relative to the mean cell count in each TME
792 large scale region (*Void, TAMM/Oligo, TAMM/vascularized)*, both in boxplot (**b**) and table (**c**)
793 formats. In **(b)** each point represents a mouse, *n*=7. For DMG cell count: *TAMM/Oligo* versus
794 *Void,* P < 0.01 (**); *TAMM/Oligo* versus *TAMM/vascularized*, P < 0.05 (*). For Iba1 cell count:
795 *TAMM/Oligo* versus *Void*, P < 0.001 (***); *TAMM/vascularized* versus *Void*, P < 0.001 (***).
796 In Olig2 cell count: *TAMM/Oligo* versus *Void,* P < 0.001 (***); *TAMM/Oligo* versus
797 *TAMM/vascularized*, P < 0.001 (***). For CD31 cell count: *TAMM/Oligo* versus *Void,* P <
798 0.001 (***); *TAMM/vascularized* versus *Void,* P < 0.001 (***); *TAMM/Oligo* versus
799 *TAMM/vascularized*, P < 0.001 (***). **d,** Boxplots showing the percentages of different DMG
800 behavioral clusters in *Void, TAMM/Oligo and TAMM/vascularized* TME large-scale regions.
801 Each point represents a different imaging position. Color: *n* = 18 independent positions; Shape:
802 *n*=6 mice. **e, f, g,** Violin plots showing DMG single cell features (*Tumor cell speed* (µm/hour)
803 (**e**), *Average speed displacement* (**f**) *and Tumor cell velocity* (µm/hour)(**g**)) differences among
804 *Void, TAMM/Oligo and TAMM/vascularized* TME large-scale regions. **e,** *TAMM/vascularized*
805 versus *Void*, P < 0.01 (**); *TAMM/vascularized* versus *TAMM/Oligo*, P < 0.01 (**). **g,** Tumor
806 cell velocity can be either towards brain core (down, negative values) or towards brain
807 parenchyma (up, positive values). For **e, f, g:** *n* = 18 independent positions from *n*=6 mice.

808 **Figure supplement 6: Cell distribution and behavioral clusters in small-scale TME. a, b,**
809 Representative 3D IVM rendering of *DMG nuclei* (cyan), CD31+ cells (grey) and SR101+ (**a**,
810 red) or CD20r+ cells (**b**, red). Scale bars, 100 µm. **c, d,** Boxplot showing *Average distance to*
811 *the 10 closest DMG neighbors (µm)* (**c**) and *Number of SR101+ cells in a 30 µm radius* (**d**)
812 across distinct DMG single-cell behavioral clusters. Each point represents an individual tracked

813 cell, color depicts the imaged position and the shape denotes the mouse. P-values represent the
814 significance of differences across behavioral clusters tested through ANOVA followed by
815 Tukey's post hoc test. $P < 0.05$ (*);$P < 0.01$ (**); $P < 0.1$ (·). **c,** n=18 independent positions
816 imaged in 6 mice. **d,** n=8 independent positions imaged in 3 mice.

817 **Supplementary video 1: BEHAV3D Tumor Profiler pipeline main characteristics and**
818 **walkthrough**. Summary video of BEHAV3D TP pipeline.

819 **Supplementary video 2: Representative intravital time-lapse video of DMG cells.** Raw
820 DMG cells time-lapse (right panel). Cell tracks were classified according to DMG behavior
821 (right panel, color coded by cluster). Representative movie from n=18 independent positions
822 imaged in 6 mice. Scale bars 40 µm.

823 **Supplementary video 3: Dynamic multispectral representative time-lapse video of DMG**
824 **cells and CD20r+ TAMM.** Time-lapse showing the movement of DMG cells (grey) relative
825 to CD20r+ TAMM (blue). The trajectories towards the TAMM of two DMG cells show a path
826 from the initial (blue) to the final position (red). Left: Tumor edge; right: tumor core.
827 Representative movie from n=10 independent positions imaged in 3 mice. Scale bars 10 µm, 7
828 µm after zoom in.

829

REFERENCES

1. Vitale, I., Shema, E., Loi, S. & Galluzzi, L. Intratumoral heterogeneity in cancer progression and response to immunotherapy. *Nat Med* **27**, 212–224 (2021).

2. Lawson, D. A., Kessenbrock, K., Davis, R. T., Pervolarakis, N. & Werb, Z. Tumour heterogeneity and metastasis at single-cell resolution. *Nat. Cell Biol.* **20**, 1349–1360 (2018).

3. Elhanani, O., Ben-Uri, R. & Keren, L. Spatial profiling technologies illuminate the tumor microenvironment. *Cancer Cell* **41**, 404–420 (2023).

4. Scheele, C. L. G. J., Maynard, C. & Rheenen, J. van. Intravital Insights into Heterogeneity, Metastasis, and Therapy Responses. *Trends Cancer* **2**, 205–216 (2016).

5. Entenberg, D., Oktay, M. H. & Condeelis, J. S. Intravital imaging to study cancer progression and metastasis. *Nat. Rev. Cancer* **23**, 25–42 (2023).

6. Alieva, M., Ritsma, L., Giedt, R. J., Weissleder, R. & Rheenen, J. van. Imaging windows for long-term intravital imaging. *IntraVital* **3**, e29917 (2014).

7. Alieva, M. *et al.* Intravital imaging of glioma border morphology reveals distinctive cellular dynamics and contribution to tumor cell invasion. *Sci. Rep.* **9**, 2054 (2019).

8. Alieva, M. & Rios, A. C. Longitudinal Intravital Imaging of Brain Tumor Cell Behavior in Response to an Invasive Surgical Biopsy. *J. Vis. Exp.* (2019) doi:10.3791/59278.

9. Zomer, A., Croci, D., Kowal, J., Gurp, L. van & Joyce, J. A. Multimodal imaging of the dynamic brain tumor microenvironment during glioblastoma progression and in response to treatment. *iScience* **25**, 104570 (2022).

10. Alieva, M. *et al.* Preventing inflammation inhibits biopsy-mediated changes in tumor cell behavior. *Sci. Rep.* **7**, 7529 (2017).

11. Janssen, A., Beerling, E., Medema, R. & Rheenen, J. van. Intravital FRET Imaging of Tumor Cell Viability and Mitosis during Chemotherapy. *PLoS ONE* **8**, e64029 (2013).

12. Croci, D., Zomer, A., Kowal, J. & Joyce, J. A. Cranial imaging window implantation technique for longitudinal multimodal imaging of the brain environment in live mice. *STAR Protoc.* **4**, 102197 (2023).

13. Zomer, A. *et al.* Brief Report: Intravital Imaging of Cancer Stem Cell Plasticity in Mammary Tumors. *STEM CELLS* **31**, 602–606 (2013).

14. Zomer, A. *et al.* In Vivo Imaging Reveals Extracellular Vesicle-Mediated Phenocopying of Metastatic Behavior. *Cell* **161**, 1046–1057 (2015).

15. Chen, N., Ritsma, L. M. A. & Vrisekoop, N. In vivo characteristics of human and mouse breast tumor cell lines. *Exp. Cell Res.* **381**, 86–93 (2019).

16. Bayarmagnai, B., Perrin, L., Pourfarhangi, K. E. & Gligorijevic, B. Cell Migration, Methods and Protocols. *Methods Mol. Biol.* **1749**, 175–193 (2018).

17. Shannon, M. J., Eisman, S. E., Lowe, A. R., Sloan, T. & Mace, E. M. cellPLATO: an unsupervised method for identifying cell behaviour in heterogeneous cell trajectory data. *J. Cell Sci.* **137**, jcs261887.

18. Crainiciuc, G. *et al.* Behavioural immune landscapes of inflammation. *Nature* **601**, 415–421 (2022).

19. Dekkers, J. F. *et al.* Uncovering the mode of action of engineered T cells in patient cancer organoids. *Nat. Biotechnol.* **41**, 60–69 (2023).

20. Freckmann, E. C. *et al.* Traject3d allows label-free identification of distinct co-occurring phenotypes within 3D culture by live imaging. *Nat. Commun.* **13**, 5317 (2022).

21. Alieva, M. *et al.* BEHAV3D: a 3D live imaging platform for comprehensive analysis of engineered T cell behavior and tumor response. *Nat. Protoc.* 1–33 (2024) doi:10.1038/s41596-024-00972-6.

22. Pizzagalli, D. U. *et al.* Leukocyte Tracking Database, a collection of immune cell tracks from intravital 2-photon microscopy videos. *Sci. Data* **5**, 180129 (2018).

23. Pizzagalli, D. U. *et al.* CANCOL, a Computer-Assisted Annotation Tool to Facilitate Colocalization and Tracking of Immune Cells in Intravital Microscopy. *J. Immunol.* **208**, 1493–1499 (2022).

24. Joseph, A., Chu, C. J., Feng, G., Dholakia, K. & Schallek, J. Label-free imaging of immune cell dynamics in the living retina using adaptive optics. *eLife* **9**, e60547 (2020).

25. Molina-Moreno, M. *et al.* ACME: Automatic feature extraction for cell migration examination through intravital microscopy imaging. *Méd. Image Anal.* **77**, 102358 (2022).

26. Hidalgo-Cenalmor, I. *et al.* DL4MicEverywhere: deep learning for microscopy made flexible, shareable and reproducible. *Nat. Methods* **21**, 925–927 (2024).

27. Ershov, D. *et al.* TrackMate 7: integrating state-of-the-art segmentation algorithms into tracking pipelines. *Nat Methods* **19**, 829–832 (2022).

28. Buczkowicz, P., Bartels, U., Bouffet, E., Becher, O. & Hawkins, C. Histopathological spectrum of paediatric diffuse intrinsic pontine glioma: diagnostic and therapeutic implications. *Acta Neuropathol.* **128**, 573–581 (2014).

29. Gómez-de-Mariscal, E. *et al.* CellTracksColab — A platform for compiling, analyzing, and exploring tracking data. *bioRxiv* 2023.10.20.563252 (2024) doi:10.1101/2023.10.20.563252.

30. Chamier, L. von *et al.* Democratising deep learning for microscopy with ZeroCostDL4Mic. *Nat Commun* **12**, 2276 (2021).

31. Dawson, C. A. *et al.* Hormone-responsive progenitors have a unique identity and exhibit high motility during mammary morphogenesis. *Cell Rep.* **43**, 115073 (2024).

32. Pachitariu, M. & Stringer, C. Cellpose 2.0: how to train your own model. *Nat. Methods* **19**, 1634–1641 (2022).

33. Archit, A. *et al.* Segment Anything for Microscopy. *Nat. Methods* **22**, 579–591 (2025).

901 34. Dawson, C. A., Mueller, S. N., Lindeman, G. J., Rios, A. C. & Visvader, J. E. Intravital micros-
902 copy of dynamic single-cell behavior in mouse mammary tissue. *Nat. Protoc.* **16**, 1907–1935 (2021).

903 35. Jung, E. *et al.* Tumor cell plasticity, heterogeneity, and resistance in crucial microenvironmental
904 niches in glioma. *Nat. Commun.* **12**, 1014 (2021).

905 36. Crainiciuc, G. *et al.* Behavioural immune landscapes of inflammation. *Nature* 1–7 (2022)
906 doi:10.1038/s41586-021-04263-y.

907 37. Jarade, A. *et al.* Inflammation triggers ILC3 patrolling of the intestinal barrier. *Nat. Immunol.* **23**,
908 1317–1323 (2022).

909 38. Chauveau, A. *et al.* Visualization of T Cell Migration in the Spleen Reveals a Network of Peri-
910 vascular Pathways that Guide Entry into T Zones. *Immunity* **52**, 794-807.e7 (2020).

911 39. Kienle, K. *et al.* Neutrophils self-limit swarming to contain bacterial growth in vivo. *Science* **372**,
912 (2021).

913 40. Liu, B. *et al.* Affinity-coupled CCL22 promotes positive selection in germinal centres. *Nature* **592**,
914 133–137 (2021).

915 41. Persson, M. L. *et al.* The intrinsic and microenvironmental features of diffuse midline glioma: Im-
916 plications for the development of effective immunotherapeutic treatment strategies. *Neuro-Oncol.* **24**,
917 1408–1422 (2022).

918 42. Ineveld, R. L. van *et al.* Multispectral confocal 3D imaging of intact healthy and tumor tissue us-
919 ing mLSR-3D. *Nat. Protoc.* **17**, 3028–3055 (2022).

920 43. Ineveld, R. L. van *et al.* Revealing the spatio-phenotypic patterning of cells in healthy and tumor
921 tissues with mLSR-3D and STAPL-3D. *Nat. Biotechnol.* **39**, 1239–1245 (2021).

922 44. Stoltzfus, C. R. *et al.* CytoMAP: A Spatial Analysis Toolbox Reveals Features of Myeloid Cell
923 Organization in Lymphoid Tissues. *Cell Rep.* **31**, 107523 (2020).

924 45. Winkler, F. *et al.* Imaging glioma cell invasion in vivo reveals mechanisms of dissemination and
925 peritumoral angiogenesis. *Glia* **57**, 1306–1315 (2009).

926 46. Wallmann, T. *et al.* Microglia Induce PDGFRB Expression in Glioma Cells to Enhance Their Mi-
927 gratory Capacity. *iScience* **9**, 71–83 (2018).

928 47. Seano, G. & Jain, R. K. Vessel co-option in glioblastoma: emerging insights and opportunities. *An-*
929 *giogenesis* **23**, 9–16 (2020).

930 48. Ravin, R. *et al.* Perivascular invasion of primary human glioblastoma cells in organotypic human
931 brain slices: human cells migrating in human brain. *J. Neuro-Oncol.* **164**, 43–54 (2023).

932 49. Gupta, R. K. *et al.* Tumor-specific migration routes of xenotransplanted human glioblastoma cells
933 in mouse brain. *Sci. Rep.* **14**, 864 (2024).

934 50. Nimmerjahn, A., Kirchhoff, F., Kerr, J. N. D. & Helmchen, F. Sulforhodamine 101 as a specific
935 marker of astroglia in the neocortex in vivo. *Nat. Methods* **1**, 31–37 (2004).

936 51. Appaix, F. *et al.* Specific In Vivo Staining of Astrocytes in the Whole Brain after Intravenous In-
937 jection of Sulforhodamine Dyes. *PLoS ONE* **7**, e35169 (2012).

938 52. Rasmussen, R., Nedergaard, M. & Petersen, N. C. Sulforhodamine 101, a widely used astrocyte
939 marker, can induce cortical seizure-like activity at concentrations commonly used. *Sci. Rep.* **6**, 30433
940 (2016).

941 53. Hagos, L. & Hülsmann, S. Unspecific labelling of oligodendrocytes by sulforhodamine 101 de-
942 pends on astrocytic uptake via the thyroid hormone transporter OATP1C1 (SLCO1C1). *Neurosci. Lett.*
943 **631**, 13–18 (2016).

944 54. Kim, B. *et al.* Visualizing Microglia with a Fluorescence Turn-On Ugt1a7c Substrate. *Angew.*
945 *Chem. Int. Ed.* **58**, 7972–7976 (2019).

946 55. Liu, I. *et al.* The landscape of tumor cell states and spatial organization in H3-K27M mutant dif-
947 fuse midline glioma across age and location. *Nat. Genet.* **54**, 1881–1894 (2022).

948 56. Xin, T. *et al.* Oncogenic Kras induces spatiotemporally specific tissue deformation through con-
949 verting pulsatile into sustained ERK activation. *Nat. Cell Biol.* **26**, 859–867 (2024).

950 57. Venkataramani, V. *et al.* Glioblastoma hijacks neuronal mechanisms for brain invasion. *Cell* **185**,
951 2899-2917.e31 (2022).

952 58. Bera, K. *et al.* Extracellular fluid viscosity enhances cell migration and cancer dissemination. *Na-*
953 *ture* **611**, 365–373 (2022).

954 59. Gertler, F. & Condeelis, J. Metastasis: tumor cells becoming MENAcing. *Trends Cell Biol.* **21**,
955 81–90 (2011).

956 60. Kluiver, T. A., Alieva, M., Vuurden, D. G. van, Wehrens, E. J. & Rios, A. C. Invaders Exposed:
957 Understanding and Targeting Tumor Cell Invasion in Diffuse Intrinsic Pontine Glioma. *Front. Oncol.*
958 **10**, 92 (2020).

959 61. Quail, D. F. & Joyce, J. A. The Microenvironmental Landscape of Brain Tumors. *Cancer Cell* **31**,
960 326–341 (2017).

961 62. Taylor, K. R. & Monje, M. Invasive glioma cells: The malignant pioneers that follow the current.
962 *Cell* **185**, 2846–2848 (2022).

963 63. Erices, J. I. *et al.* Glioblastoma Microenvironment and Invasiveness: New Insights and Therapeutic
964 Targets. *Int. J. Mol. Sci.* **24**, 7047 (2023).

965 64. Patel, S. K. *et al.* Generation of diffuse intrinsic pontine glioma mouse models by brainstem-tar-
966 geted in utero electroporation. *Neuro-Oncol.* **22**, 381–392 (2020).

967 65. Chatinier, A. du *et al.* Generation of immunocompetent syngeneic allograft mouse models for pe-
968 diatric diffuse midline glioma. *Neuro-Oncol. Adv.* **4**, vdac079 (2022).

969 66. Srivastava, R. *et al.* Development of a human glioblastoma model using humanized DRAG mice
970 for immunotherapy. *Antib. Ther.* **6**, 253–264 (2023).

971 67. Wezenaar, A. K. L. *et al.* Mapping T cell dynamics to molecular profiles through behavior-guided
972 transcriptomics. *Nat. Protoc.* 1–28 (2025) doi:10.1038/s41596-024-01126-4.

68. Aragones, D. G. *et al.* Variable selection for nonlinear dimensionality reduction of biological datasets through bootstrapping of correlation networks. *Comput. Biol. Med.* **168**, 107827 (2024).

69. Klein, S., Staring, M., Murphy, K., Viergever, M. A. & Pluim, J. P. W. elastix: A Toolbox for Intensity-Based Medical Image Registration. *IEEE Trans. Méd. Imaging* **29**, 196–205 (2010).

70. Marstal, K., Berendsen, F., Staring, M. & Klein, S. SimpleElastix: A User-Friendly, Multi-Lingual Library for Medical Image Registration. *2016 IEEE Conf. Comput. Vis. Pattern Recognit. Work. (CVPRW)* 574–582 (2016) doi:10.1109/cvprw.2016.78.

71. Rios, A. C. *et al.* Intraclonal Plasticity in Mammary Tumors Revealed through Large-Scale Single-Cell Resolution 3D Imaging. *Cancer Cell* **35**, 618-632.e6 (2019).

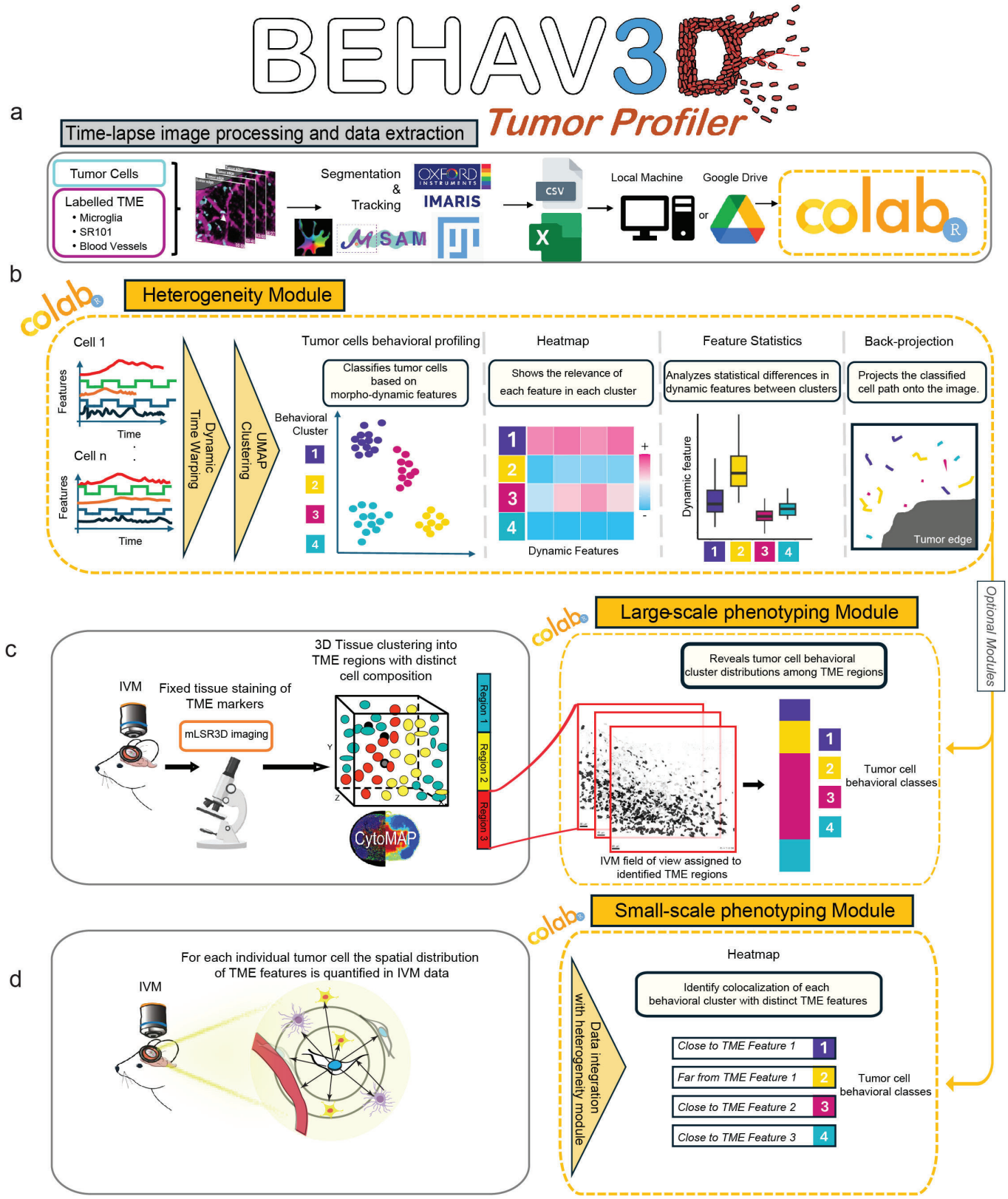
BEHAV3D
Tumor Profiler
a
Time-lapse image processing and data extraction
Tumor Cells
Labelled TME
• Microglia
• SR101
• Blood Vessels
Segmentation & Tracking
OXFORD INSTRUMENTS
IMARIS
MSAM
CSV
Local Machine
Google Drive
or
colab
b
Heterogeneity Module
Cell 1
Features
Time
Cell n
Dynamic Time Warping
UMAP Clustering
Tumor cells behavioral profiling
Classifies tumor cells based on morpho-dynamic features
Behavioral Cluster
Heatmap
Shows the relevance of each feature in each cluster
Dynamic Features
Feature Statistics
Analyzes statistical differences in dynamic features between clusters
Dynamic feature
Back-projection
Projects the classified cell path onto the image.
Tumor edge
Optional Modules
c
Large-scale phenotyping Module
IVM
Fixed tissue staining of TME markers
mLSR3D imaging
3D Tissue clustering into TME regions with distinct cell composition
CytoMAP
Region 1
Region 2
Region 3
Reveals tumor cell behavioral cluster distributions among TME regions
IVM field of view assigned to identified TME regions
Tumor cell behavioral classes
d
Small-scale phenotyping Module
For each individual tumor cell the spatial distribution of TME features is quantified in IVM data
IVM
Heatmap
Identify colocalization of each behavioral cluster with distinct TME features
Data integration with heterogeneity module
Close to TME Feature 1
Far from TME Feature 1
Close to TME Feature 2
Close to TME Feature 3
Tumor cell behavioral classes

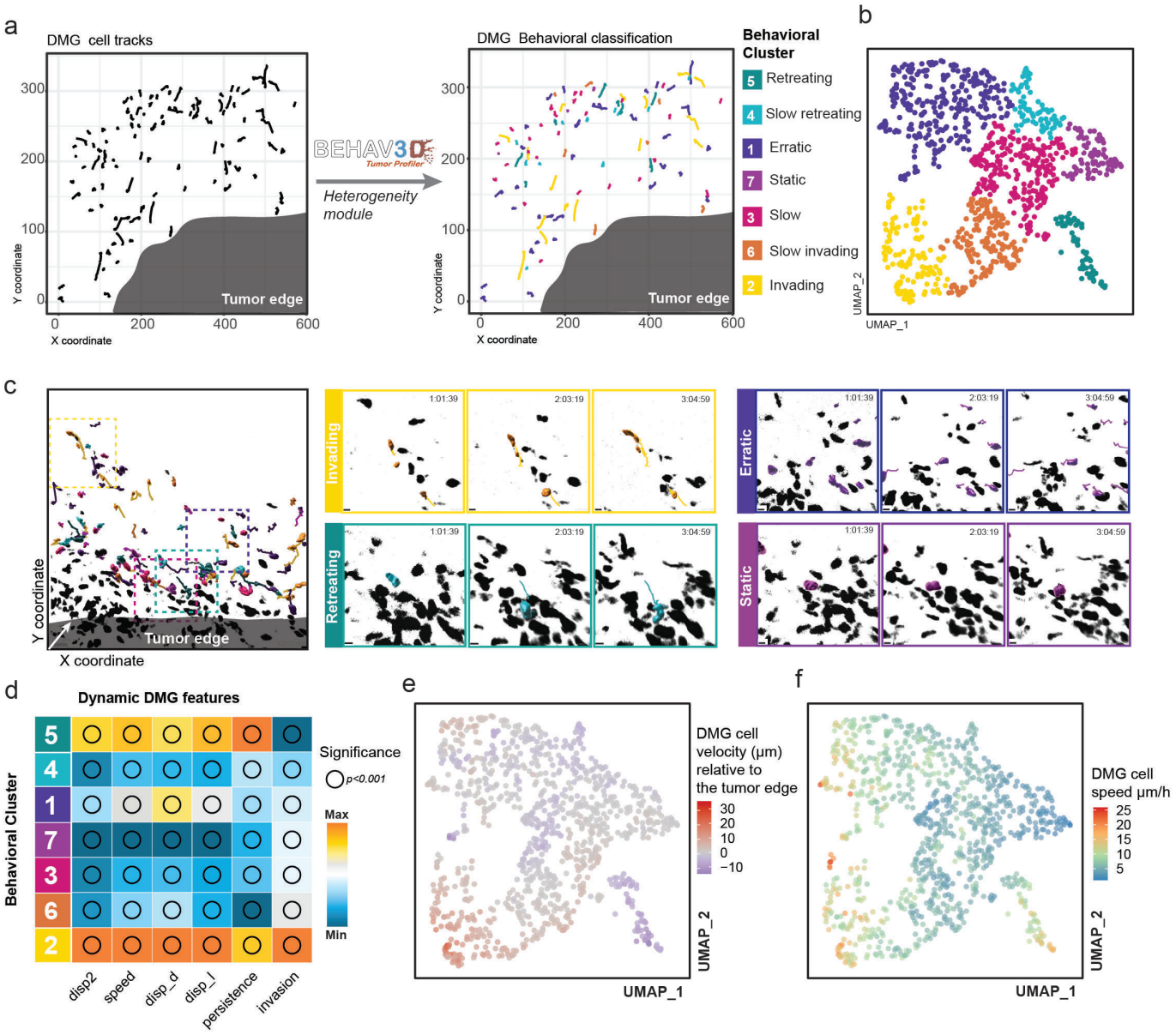

Figure 2. Behavioral profiling of DMG cells with BEHAV3D-TP heterogeneity module.

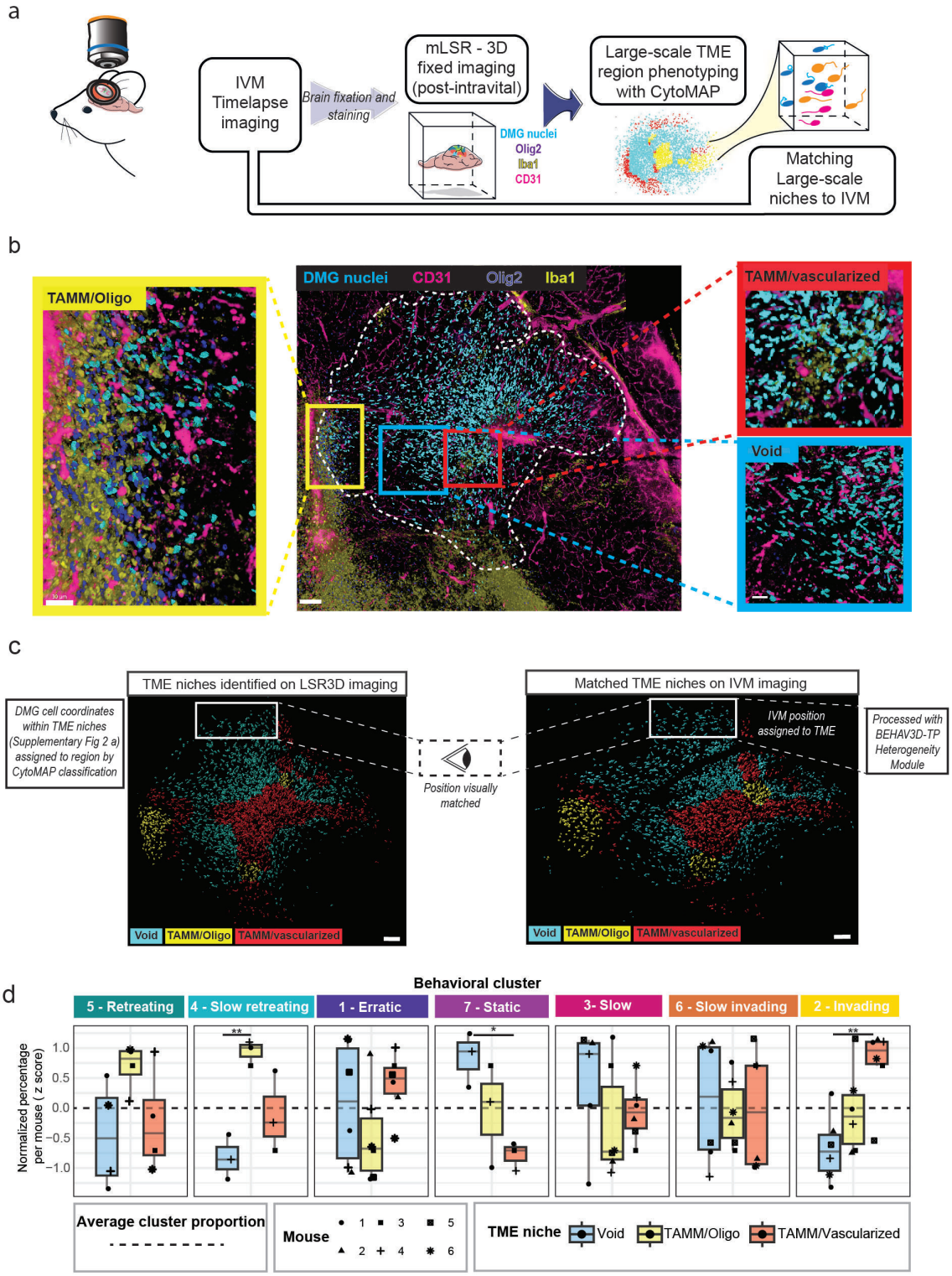

Figure 3: Mapping distinct DMG behavioral patterns to distinct TME regions

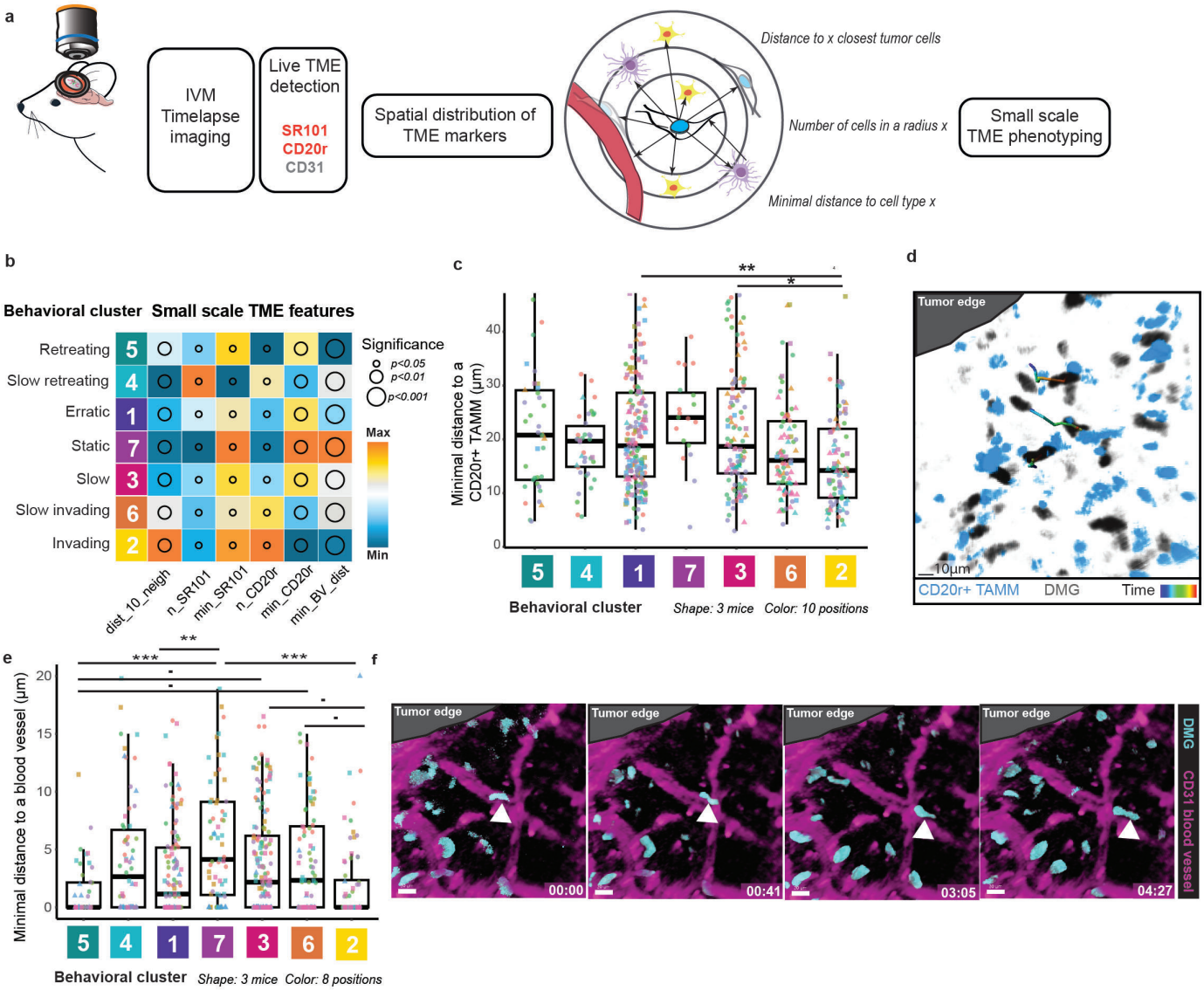

Figure 4. The BEHAV3D-TP small-scale phenotyping correlates DMG behavioral profiles with microenvironmental composition at a single-cell resolution